第5章　抗がん剤の治験業務

第6章　がん薬物療法と薬剤管理指導業務

第7章　抗がん剤の医薬品情報

第8章 国内の特殊な薬剤業務と海外の現状

LIPPINCOTT WILLIAMS & WILKINS
Reprinted in Japan

Gefitinib in the adjuvant setting: safety results from a phase III study in patients with completely resected non-small cell lung cancer

Masahiro Tsuboi[a], Harubumi Kato[a], Kanji Nagai[b], Ryosuke Tsuchiya[c], Hiromi Wada[d], Hirohito Tada[e], Yukito Ichinose[f], Masahiro Fukuoka[g] and Haiyi Jiang[h]

Standard therapy for stage I–IIIA non-small cell lung cancer (NSCLC) is surgery, although adjuvant therapies are required to prevent disease recurrence and improve patient survival. This is the first study that planned to administer adjuvant gefitinib (Iressa) 250 mg/day or placebo to randomized patients with completely resected NSCLC (stage IB–IIIA) 4–6 weeks following surgery, for 2 years, until recurrence/withdrawal. However, recruitment was stopped after the randomization of 38 patients, because interstitial lung disease (ILD)-type events were being increasingly reported in Japan in the advanced disease setting. Finally, the trial was halted. Safety data for 38 recruited patients (18 gefitinib and 20 placebo) showed no unexpected adverse drug reactions (ADRs), with the most common being grade 1/2 gastrointestinal and skin disorders in 12 and 16 patients receiving gefitinib and in five and six patients receiving placebo, respectively. Grade 3/4 ADRs occurred in four patients receiving gefitinib and one patient receiving placebo. ILD-type events were reported in one patient receiving gefitinib (concomitantly with other ILD-inducing drugs) who died and two patients receiving placebo. Eight patients receiving gefitinib withdrew due to ADRs compared with three patients receiving placebo. Adverse events associated with surgical complications were reported for six patients receiving gefitinib and four patients receiving placebo. In the adjuvant setting there were no unexpected adverse events observed. Gefitinib had no impact on surgery-related complications when given within 4–6 weeks post-operatively. *Anti-Cancer Drugs* **16:1123–1128 © 2005 Lippincott Williams & Wilkins.**

Anti-Cancer Drugs 2005, 16:1123–1128

Keywords: gefitinib, non-small cell lung cancer, phase III, safety

[a]Tokyo Medical University Hospital, Tokyo, Japan, [b]National Cancer Center Hospital East, Chiba, Japan, [c]National Cancer Center Hospital, Tokyo, Japan, [d]Kyoto University Faculty of Medicine, Kyoto, Japan, [e]Osaka City General Hospital, Osaka, Japan, [f]National Kyushu Cancer Center, Fukuoka, Japan, [g]Kinki University School of Medicine, Osaka, Japan and [h]AstraZeneca KK, Osaka, Japan.

Sponsorship: This trial was coordinated and supervised by the Study Coordinating Committee (principal investigators plus AstraZeneca personnel), and the Independent Data Monitoring Committee (lung cancer and statistical experts independent of AstraZeneca), with funding and organizational support from the trial sponsor AstraZeneca.

Correspondence to M. Tsuboi, Department of Surgery, Tokyo Medical University Hospital, 6-7-1 Nishi-Shinjuku, Shinjuku-ku, Tokyo 160-0023, Japan.
Tel: +81-3-3342-6111; fax: +81-3-3349-0326;
e-mail: mtsuboi@za2.so-net.ne.jp

Received 21 February 2005 Revised form accepted 3 August 2005

Introduction

Non-small cell lung cancer (NSCLC) is generally not diagnosed until the disease is symptomatic, by which time more than two-thirds of patients are in the advanced stages of disease and have a poor prognosis [1]. Approximately 25% of patients with NSCLC are diagnosed when their disease is in the early stages; however, as many of these patients frequently have undetectable metastases, disease often recurs in distant sites [2]. Adjuvant therapies are therefore required to help prevent disease recurrence and as they will need to be given to patients post-operatively for a prolonged period, they should be well tolerated.

Although some clinical trials in NSCLC have shown a significant survival benefit with adjuvant uracil plus tegafur (UFT) and cisplatin-based chemotherapy [3–7], others have not observed a significant improvement in survival [5,8,9]. At the time of commencing this study, there were no standard adjuvant treatment regimens for NSCLC.

Gefitinib (Iressa), an orally active epidermal growth factor receptor tyrosine kinase inhibitor (EGFR-TKI), was approved in Japan for the treatment of inoperable or recurrent NSCLC in 2002. Two large phase II trials, IDEAL (Iressa Dose Evaluation in Advanced Lung cancer) 1 and 2, observed objective responses and stable disease in more than 40% of pre-treated patients with NSCLC receiving 250 mg/day gefitinib, with the majority of adverse events (AEs) being mild to moderate gastrointestinal and skin disorders [10,11]. Gefitinib was not associated with the well-recognized AEs observed with cytotoxic chemotherapy (e.g. bone marrow depression, neurotoxicity, nephrotoxicity). The tolerability profile of gefitinib has been confirmed by data from the

Expanded Access Programme, through which more than 39 000 patients have received gefitinib 250 mg/day on a compassionate-use basis. Furthermore, a retrospective analysis of 9515 US patients who had received gefitinib for 1 year or more via the Expanded Access Programme showed a 1-year survival rate of 33% [12], which compares with the IDEAL studies [10,11]. Recently, Onn *et al.* observed efficacy (16% with objective responses and 45% with stable disease) and a low incidence of grade 3/4 AEs in Japanese patients with NSCLC, most of whom had been treated with second-line gefitinib or above (99% of patients) [13].

To date, there is no experience of using gefitinib in the post-operative adjuvant setting. This phase III trial was initially undertaken to compare survival rates in patients with completely resected stage IB–IIIA NSCLC who had been treated with adjuvant gefitinib 250 mg/day or placebo. However, in October 2002, recruitment was halted following high-profile media activity around reports of gefitinib-related interstitial lung disease (ILD)-type events in patients with advanced or metastatic NSCLC in Japan. In March 2003, the trial was halted because of an increased withdrawal rate. As enrollment could not be resumed until the prospective investigation into gefitinib-related ILD-type events in Japan was completed, the trial was closed. Consequently survival data are not available, although data from patients recruited to the study have been subsequently analyzed for safety.

Fig. 1

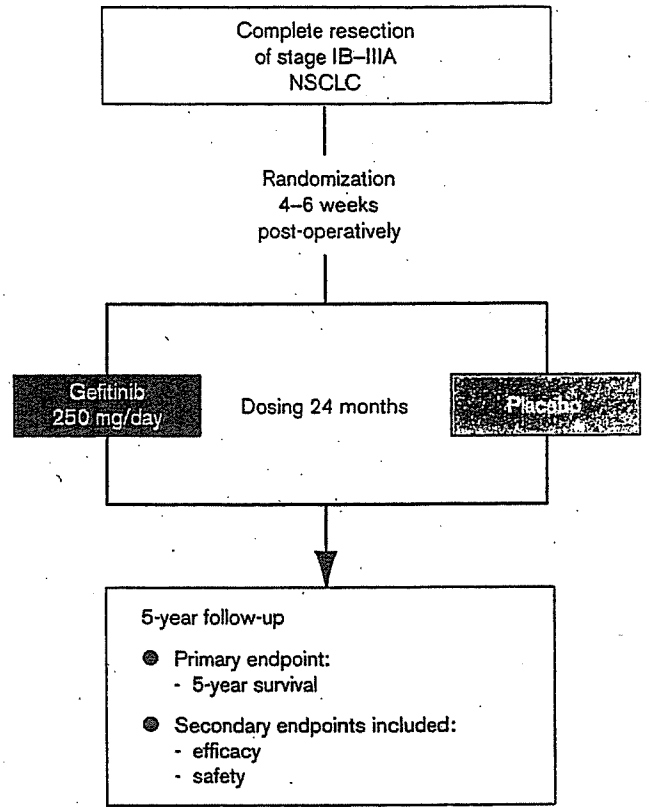

Trial design schema.

Methods

Patients

Patients were eligible for inclusion in the trial if they had histologically confirmed NSCLC (post-operative stage IB–IIIA) that had been completely resected 4–6 weeks before the start of treatment. Patients were required to be 20–75 years of age, with a WHO performance status (PS) 0–1, no previous history of chemotherapy, radiotherapy or immunotherapy for NSCLC and no co-malignancies within the past 5 years. All patients gave written, informed consent to participate in the trial, which was conducted in accordance with the Declaration of Helsinki [14] and Good Clinical Practice guidelines.

Study design

This randomized (1:1), double-blind, placebo-controlled, phase III multicenter survival study planned to recruit 670 patients (335 per group) and randomize them to receive either gefitinib (250 mg) or placebo (Fig. 1). Treatment was to be continued for 2 years, or until recurrence/secondary carcinoma or withdrawal criteria were met. An Independent Data Monitoring Committee (IDMC) was set up to assess the efficacy and safety of gefitinib post-operatively, and would advise whether the study should be continued, changed or discontinued.

Assessments

Efficacy

Disease recurrence or secondary carcinogenesis were assessed using X-rays every 3 months during treatment and every 6 months during the follow-up period. Computed tomography (CT) scans were carried out 8 weeks after the first dose (where necessary, the pre-operative thoracoabdominal CT scan could be used), at week 48 during treatment, at week 104 after withdrawal/completion and every 52 weeks thereafter, unless disease recurrence was observed.

Safety

AEs were to be recorded and coded using MedDRA (Medical Dictionary for Regulatory Activities) version 6.0, graded using National Cancer Institute Common Toxicity Criteria (NCI-CTC) version 2.0 and assigned causality by the investigators. AEs associated with post-operative complications were defined as events occurring within 90 days after surgery and were recorded without regard to causality. Treatment could be interrupted for up to 14 days, although the IDMC later recommended that drug interruption could be allowed for more than 14 days in cases where ILD-type events were suspected, but could not be confirmed, in order to ensure the safety of

patients who remained in the trial after recruitment was halted. Hematology, biochemistry and urinalysis were also measured at baseline and during the study.

Role of the funding source

This trial was coordinated and supervised by the principal investigators, the IDMC and AstraZeneca personnel, with funding and organizational support from the trial sponsor AstraZeneca.

Results

Patients

Between August and October 2002, 38 patients were randomized into the trial – 18 received gefitinib and 20 received placebo. Patient demography was well balanced between the treatment arms, with the majority of patients having adenocarcinoma histology and WHO PS 1 (Table 1). When the trial was stopped, four patients in the gefitinib arm and 11 patients in the placebo arm were still receiving treatment (Fig. 2). Of the 23 patients who withdrew, 13 did so because of AEs (10 in the gefitinib arm and three in the placebo arm), five were unwilling to continue with treatment (three in the gefitinib arm and two in the placebo arm), two had disease recurrence (both in the placebo arm) and three withdrew for other reasons (one patient in the gefitinib arm had incomplete recovery from surgery that was not drug related, and two patients in the placebo arm had pre-existing interstitial pneumonia and were withdrawn at the request of the sponsor).

Table 1 Patient demography

	Gefitinib 250 mg/day (n=18)	Placebo (n=20)
Sex [n (%)]		
male	14 (77.8)	15 (75.0)
female	4 (22.2)	5 (25.0)
Median age [years (range)]	64.0 (49–73)	62.5 (52–73)
WHO PS [n (%)]		
0	5 (27.8)	9 (45.0)
1	13 (72.2)	11 (55.0)
Histology [n (%)]		
squamous cell carcinoma	4 (22.2)	6 (30.0)
adenocarcinoma	14 (77.8)	14 (70.0)
Stage [n (%)]		
IB	7 (38.9)	8 (40.0)
IIA	2 (11.1)	1 (5.0)
IIB	3 (16.7)	5 (25.0)
IIIA	6 (33.3)	6 (30.0)

Efficacy

From the limited efficacy data, disease recurrence was not seen in patients receiving gefitinib at data cutoff. Three patients who received placebo (one with stage IB and two with stage IIB) experienced disease recurrence – two patients recurred during the trial and one patient recurred after the trial had stopped.

ADRs

No unexpected ADRs were observed and, in general, the frequency of all ADRs was higher for gefitinib versus placebo (Table 2). The most common ADRs were mild to moderate grade 1/2 gastrointestinal and skin disorders. Grade 3/4 ADRs were seen in four patients in the gefitinib arm and one patient in the placebo arm (Table 3), all of whom had treatment withdrawn (the patient with grade 3 eczema had treatment withdrawn due to grade 2 impetigo).

Respiratory ADRs

The majority of respiratory ADRs were grade 1/2 and occurred within 1 month of treatment. In the gefitinib arm, two patients experienced cough (associated with post-operative complications), one patient had dyspnea,

Fig. 2

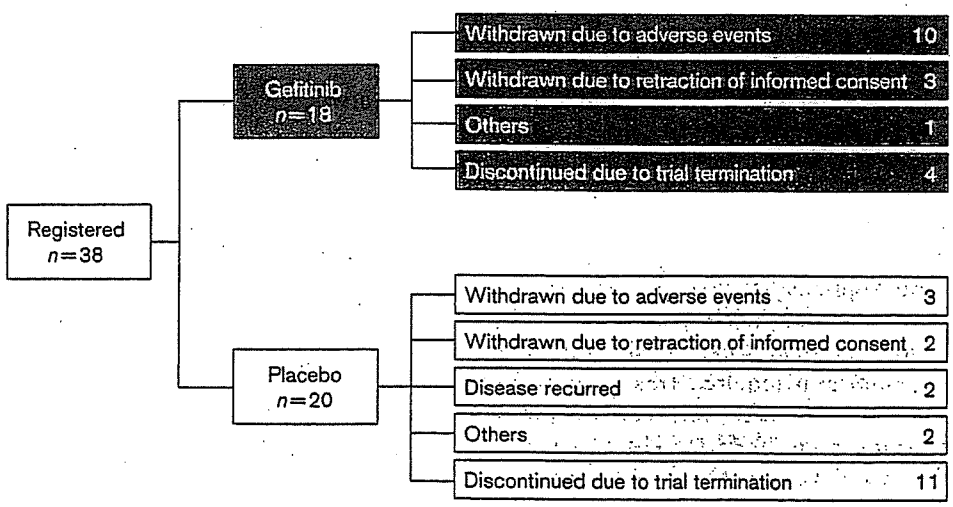

Trial outcome.

Table 2 Common ADRs occurring in two or more patients

AE (MedDRA term)[a]	Gefitinib 250 mg/day ($n=18$)	Placebo ($n=20$)
Abnormal hepatic function	4	0
Acne	2	0
Anorexia	5	1
Cough	2[b]	1
Diarrhea	9	2
Dry skin	3	0
Eczema	8	2
Elevated ALT/AST	2	0
Fatigue	2	0
Gastritis	3[b]	0
Loose stools	4	0
Nausea	3	0
Rash	5	3
Sputum	0	2
Stomatitis	2	0

[a]A patient could have more than one AE.
[b]All were associated with post-operative complications.

Table 3 Grade 3/4 ADRs

AE (MedDRA term)	Grade	Gefitinib 250 mg/day ($n=18$)	Placebo ($n=20$)
Abnormal hepatic function	3	1	0
Eczema	3	1	0
Elevated ALT	3	1	0
Neutropenia	3	0	1
Pneumonitis	4	1	0

Table 4 Exposure of patients to gefitinib

	Gefitinib 250 mg/day ($n=18$)	Placebo ($n=20$)
Median duration of treatment [days (range)]	86.5 (4–195)	144.0 (20–197)
Dosing period (n)		
<60 days	6	2
60–120 days	9	4
≥ 120 days	3	14
No. dose interruptions (n)		
1	5	6
2	2	2
≥ 3	2	2

Table 5 ADRs leading to patient withdrawals

Adverse event (MedDRA term)	Grade	Gefitinib 250 mg/day ($n=18$)	Placebo ($n=20$)
Eczema	2	1	0
Elevated ALT/AST	2	1	0
	3	1	0
Hepatic function abnormalities	2	1	0
	3	1	0
ILD	1	0	1
Impetigo	2	1	0
Neutropenia	3	0	1
Paronychia	2	1	0
Pneumonitis	4	1	0
Pulmonary fibrosis	1	0	1

and one patient experienced grade 4 ILD-type events (pneumonitis) 107 days after starting gefitinib and was withdrawn from the study. The patient with pneumonitis had taken concomitant shosaikoto, a Chinese herbal medicine, and loxoprofen, both of which have previously been shown to induce pneumonitis [15,16]. Twenty-one days later bacterial pneumonia related to methylprednisolone therapy was diagnosed, and the patient subsequently died 37 days later due to both pneumonitis and bacterial pneumonia. In the placebo arm, one patient who experienced cough and grade 1 pulmonary fibrosis had had interstitial changes on their chest X-ray at enrollment, and in a second patient, pre-existing non-specific interstitial pneumonia was exacerbated resulting in grade 1 ILD. In both patients, these conditions persisted following withdrawal of study drug.

Interruptions and withdrawals due to ADRs

ADRs requiring interruptions in therapy were similar between patients receiving gefitinib or placebo (Table 4) and were usually for less than 14 days, although four patients in the gefitinib arm required treatment to be interrupted for 14 days (including one patient whose treatment was interrupted for 20 days). The majority of ADRs leading to withdrawal were usually mild-to-moderate grade 1/2 in severity (Table 5). Grade 3 ADRs leading to withdrawal occurred in two patients receiving gefitinib (hepatic function abnormalities, elevated ALT) and in one patient receiving placebo (neutropenia), and grade 4 pneumonitis led to the withdrawal of one patient who was receiving gefitinib. Following withdrawal of gefitinib treatment, grade 3 abnormal hepatic function and elevated ALT resolved, and grade 3 neutropenia persisted.

AEs associated with post-operative complications

As there are no safety data regarding the use of gefitinib in the post-operative setting, AEs associated with the healing process were examined to provide preliminary safety data on the start of the dosing timing in the adjuvant setting for gefitinib. AEs related to post-operative complications were observed in six patients in the gefitinib arm and four patients in the placebo arm. In the gefitinib arm, the most frequent AEs were grade 1/2 cough (four patients) and gastritis (three patients), and in the placebo arm grade 1/2 pain (three patients). Grade 1 cough, grade 1 supraventricular arrhythmia and grade 2 dyspnea were also experienced by three out of four patients receiving placebo.

Discussion

This trial was designed to compare survival rates in patients with completely resected stage IB–IIIA NSCLC who had received adjuvant therapy with gefitinib 250 mg/day or placebo. However, incidences of ADRs of ILD-

type events in the advanced disease setting have been increasingly reported since gefitinib was launched in Japan, and new recruitment was put on hold on 23 October 2002 at the request of the Ministry of Health, Labor and Welfare. In order to evaluate the ILD and ensure the safety of the trial patients, two separate Co-ordination Committee and IDMC meetings (December 2002 and January 2003) were conducted to discuss the feasibility of continuing the study and management of the trial patients. Based on the updated information on ADRs of interstitial pneumonia, the committees concluded that the study could be continued because the possibility of risk did not exceed that of benefit to enrolled patients. The IDMC also suggested that top priority should be given to assure the safety of the patients receiving gefitinib, and that discontinuation should be considered if flu-like symptoms including difficulty in breathing, fever and coughing occurred.

A 'Supplemental Explanation Sheet and Informed Consent Form' was provided four times to enrolled patients, offered updated information and methods to assure and manage any safety issues, and confirmed the patients' willingness to continue participating in the study. In December 2002, AstraZeneca KK gave the principal investigators the option to suspend gefitinib treatment at once. With the extensive monitoring of the trial patients in terms of safety, there were still an increasing number of withdrawals. In addition, enrollment could not be resumed until the prospective investigation on gefitinib-related ILD was completed. Based on these facts, the sponsor finally decided to terminate the trial in March 2003.

The types of AEs reported in this trial were similar to that already reported in the large phase II IDEAL 1 and 2 trials for patients with locally advanced or metastatic NSCLC [10,11]. Three patients experienced ILD-type events – two in the placebo arm and one patient in the gefitinib arm (this patient was also taking two other medications known to induce ILD) [15,17]. It has generally been observed that a higher frequency of ILD-type events are reported in Japanese patients taking gefitinib compared with those in other south-east Asian countries and the rest of the world (1.6, 0.3, and 0.3%, respectively) [18]. The occurrence of ILD in Japanese patients and the reasons for such an ethnic stratification in ILD incidence following gefitinib treatment require further clarification.

The most common reason for withdrawal in both treatment arms was due to toxicity, with the majority of drug-related AEs being grade 1/2 in severity. In the advanced or metastatic disease setting, few patients who experience grade 1/2 drug-related AEs withdraw from treatment with gefitinib, and in IDEAL 1, which recruited Japanese patients, two out of 103 patients who received gefitinib 250 mg/day withdrew from therapy due to ADRs [18]. Several factors may explain the high number of withdrawals (including withdrawal of treatment for less severe ADRs) reported in this trial data compared with previously reported studies. These reasons include the fact that patients with early-stage NSCLC may be less tolerant of AEs compared with patients with advanced NSCLC who have received prior chemotherapy. In contrast to the other studies, the impact of heavy media coverage surrounding gefitinib-related ILD cannot be ignored.

It has been suggested that the dosage and schedule of gefitinib used in this study may not best suit patients with completely resected NSCLC in terms of tolerability and a number of adjustments may need to be taken into consideration when planning an adjuvant study of gefitinib in the future. It is unlikely that the time frame of 4–6 weeks is too short before starting adjuvant treatment, as other adjuvant trials conducted in Japanese patients have used similar time frames [3,4]. It may be possible to lengthen the duration by which gefitinib could be interrupted for toxicity, since 14 days may be too short for patients recovering from AEs such as hepatic enzyme elevation, or to reduce the dose following toxicity to perhaps 250 mg every other day, although this would require further study into the efficacy of such an approach.

With no experience of using gefitinib in post-operative patients there was a concern that EGFR-TKIs might impact on surgery-related complications (especially on the healing process) due to their mode of action. In order to assess this, the trial was designed to allow a safety review of the first 60 patients. Due to the early termination of the study, we have only 38 patients' (18 on gefitinib) data for review; however, there does not seem to be any impact on surgery-related complications when gefitinib was administered within 4–6 weeks after surgery, as evidenced by a similar number of these AEs that occurred in both groups. This indicates that it may be feasible to administer gefitinib in the adjuvant setting within this time frame.

In conclusion, this is the first study to investigate the use of EGFR-TKIs as adjuvant therapy. Despite the absence of survival data, there were no unexpected AEs seen in the adjuvant setting compared with those already reported for patients with locally advanced or metastatic NSCLC. However, it was observed that there were more AEs leading to withdrawal in the gefitinib arm, even though the majority of AEs were grade 1/2 in severity, suggesting that a daily dose of gefitinib 250 mg may not best suit patients with completely resected NSCLC in terms of tolerability.

Acknowledgements

The following individuals are the principle investigators and IDMC members: Tetsuya Mitsudomi, Aichi Cancer Center, Nagoya; Motoi Aoe, Okayama University School of Medicine, Okayama; Hideyuki Saeki, National Shikoku Cancer Center, Ehime; Katsuhiro Nakagawa, Osaka Prefectural Habikino Hospital, Osaka; Teruaki Koike, Niigata Cancer Center Hospital, Niigata; Chiaki Endo, Tohoku University School of Medicine, Sendai; Makoto Oda, Kanazawa University School of Medicine, Kanazawa; Kohei Yokoi, Tochigi Cancer Center, Tochigi; Toshihiko Iizasa, Chiba University School of Medicine, Chiba; Fumihiro Tanaka, Kyoto University Faculty of Medicine, Kyoto; Akihide Matsumura, National Kinki Chuo Hospital, Osaka; Ichiro Yoshino, Kyusyu University School of Medicine, Fukuoka; Nagahiro Saijo, National Cancer Center, Tokyo; Haruhiko Fukuda, National Cancer Center, Tokyo; Naoki Ishizuka, National Cancer Center, Tokyo; Tomoyuki Goya, Kyorin University Hospital, Tokyo; Ryuzo Ueda, Nagoya University School of Medicine, Nagoya. We thank Dr Carolyn Gray, from Complete Medical Communications, who provided medical writing support on behalf of AstraZeneca. Iressa is a trademark of the AstraZeneca group of companies

References

1 Ries LAG, Eisner MP, Kosary CL, Hankey BF, Miller BA, Clegg L, *et al. SEER cancer statistics review*; 2004. http://seer.cancer.gov/csr/1975_2001/.

2 Martini N, Bains MS, Burt ME, Zakowski MF, McCormack P, Rusch VW, *et al.* Incidence of local recurrence and second primary tumors in resected stage I lung cancer. *J Thorac Cardiovasc Surg* 1995; **109**:120–129.

3 Kato H, Ichinose Y, Ohta M, Hata E, Tsubota N, Tada H, *et al.* A randomized trial of adjuvant chemotherapy with uracil–tegafur for adenocarcinoma of the lung. *N Engl J Med* 2004; **350**:1713–1721.

4 Wada H, Hitomi S, Teramatsu T. Adjuvant chemotherapy after complete resection in non-small-cell lung cancer. West Japan Study Group for Lung Cancer Surgery. *J Clin Oncol* 1996; **14**:1048–1054.

5 Non-Small Cell Lung Cancer Collaborative Group. Chemotherapy in non-small cell lung cancer: a meta-analysis using updated data on individual patients from 52 randomised clinical trials. *Br Med J* 1995; **311**:899–909.

6 Tanaka F, Miyahara R, Ohtake Y, Yanagihara K, Fukuse T, Hitomi S, *et al.* Advantage of post-operative oral administration of UFT (tegafur and uracil) for completely resected p-stage I–IIIa non-small cell lung cancer (NSCLC). *Eur J Cardiothorac Surg* 1998; **14**:256–262.

7 Arriagada R, Bergman B, Dunant A, Le Chevalier T, Pignon JP, Vansteenkiste J. Cisplatin-based adjuvant chemotherapy in patients with completely resected non-small-cell lung cancer. *N Engl J Med* 2004; **350**:351–360.

8 Endo C, Saito Y, Iwanami H, Tsushima T, Imai T, Kawamura M, *et al.* A randomized trial of postoperative UFT therapy in p stage I, II non-small cell lung cancer: North-east Japan Study Group for Lung Cancer Surgery. *Lung Cancer* 2003; **40**:181–186.

9 Wada H, Miyahara R, Tanaka F, Hitomi S. Postoperative adjuvant chemotherapy with PVM (Cisplatin + Vindesine + Mitomycin C) and UFT (Uracil + Tegafur) in resected stage I–II NSCLC (non-small cell lung cancer): a randomized clinical trial. West Japan Study Group for lung cancer surgery (WJSG). *Eur J Cardiothorac Surg* 1999; **15**:438–443.

10 Fukuoka M, Yano S, Giaccone G, Tamura T, Nakagawa K, Douillard J-Y, *et al.* Multi-institutional randomized phase II trial of gefitinib for previously treated patients with advanced non-small-cell lung cancer. *J Clin Oncol* 2003; **21**:2237–2246.

11 Kris MG, Natale RB, Herbst RS, Lynch Jr TJ, Prager D, Belani CP, *et al.* Efficacy of gefitinib, an inhibitor of the epidermal growth factor receptor tyrosine kinase, in symptomatic patients with non-small cell lung cancer. A randomized trial. *J Am Med Ass* 2003; **290**:2149–2158.

12 Ochs J, Grous JJ, Warner KL. Final survival and safety results for 21,064 non-small-cell lung cancer (NSCLC) patients who received compassionate use gefitinib in a U.S. expanded access program (EAP). *Proc Am Soc Clin Oncol* 2004; **23**:628.

13 Onn A, Tsuboi M, Thatcher N. Treatment of non-small-cell lung cancer: a perspective on the recent advances and the experience with gefitinib. *Br J Cancer* 2004; **91(Suppl 2)**:S11–S17.

14 World Medical Association. World Medical Association Declaration of Helsinki. Recommendations guiding physicians in biomedical research involving human subjects. *J Am Med Ass* 1997; **277**:925–926.

15 Sato A, Toyoshima M, Kondo A, Ohta K, Sato H, Ohsumi A. Pneumonitis induced by the herbal medicine Sho-saiko-to in Japan. *Nihon Kyobu Shikkan Gakkai Zasshi* 1997; **35**:391–395.

16 Tohyama M, Tamaki Y, Toyama M, Ishimine T, Miyazato A, Nakamoto A, *et al.* A case of loxoprofen-induced pneumonitis pathologically resembling hypersensitivity pneumonitis. *Nihon Kokyuki Gakkai Zasshi* 2002; **40**: 123–128.

17 Miyazaki E, Ando M, Ih K, Matsumoto T, Kaneda K, Tsuda T. [Pulmonary edema associated with the Chinese medicine shosaikoto]. *Nihon Kokyuki Gakkai Zasshi* 1998; **36**:776–780.

18 Forsythe B, Faulkner K. Overview of the tolerability of gefitinib (IRESSA™) monotherapy. Clinical experience in non-small-cell lung cancer. *Drug Safety* 2004; **27**:1081–1092.

Priority Report

Element Array by Scanning X-ray Fluorescence Microscopy after *Cis*-Diamminedichloro-Platinum(II) Treatment

Mari Shimura,[1] Akira Saito,[4,8,9] Satoshi Matsuyama,[5] Takahiro Sakuma,[1] Yasuhito Terui,[3] Kazumasa Ueno,[5] Hirokatsu Yumoto,[5] Kazuto Yamauchi,[5] Kazuya Yamamura,[6] Hidekazu Mimura,[5] Yasuhisa Sano,[5] Makina Yabashi,[7] Kenji Tamasaku,[8] Kazuto Nishio,[2] Yoshinori Nishino,[8] Katsuyoshi Endo,[6] Kiyohiko Hatake,[3] Yuzo Mori,[6] Yukihito Ishizaka,[1] and Tetsuya Ishikawa[8]

[1]Department of Intractable Diseases, International Medical Center of Japan; [2]Pharmacology Division, National Cancer Center Research Institute; [3]Division of Clinical Chemotherapy, Cancer Chemotherapy Center, Japanese Foundation for Cancer Research, Tokyo, Japan; Departments of [4]Material and Life Science and [5]Precision Science and Technology, and [6]Research Center for Ultra-Precision Science and Technology, Graduate School of Engineering, Osaka University, Suita, Osaka, Japan; [7]SPring-8/Japan Synchrotron Radiation Research Institute and [8]SPring-8/Riken, Hyogo, Japan; and [9]Nanoscale Quantum Conductor Array Project, ICORP, Saitama, Japan

Abstract

Minerals are important for cellular functions, such as transcription and enzyme activity, and are also involved in the metabolism of anticancer chemotherapeutic compounds. Profiling of intracellular elements in individual cells could help in understanding the mechanism of drug resistance in tumors and possibly provide a new strategy of anticancer chemotherapy. Using a recently developed technique of scanning X-ray fluorescence microscopy (SXFM), we analyzed intracellular elements after treatment with *cis*-diamminedichloro-platinum(II) (CDDP), a platinum-based anticancer agent. The images obtained by SXFM (element array) revealed that the average Pt content of CDDP-resistant cells was 2.6 times less than that of sensitive cells, and the zinc content was inversely correlated with the intracellular Pt content. Data suggested that Zn-related detoxification is responsible for resistance to CDDP. Of Zn-related excretion factors, glutathione was highly correlated with the amount of Zn. The combined treatment of CDDP and a Zn(II) chelator resulted in the incorporation of thrice more Pt with the concomitant down-regulation of glutathione. We propose that the generation of an element array by SXFM opens up new avenues in cancer biology and treatment. (Cancer Res 2005; 65(12): 4998-5002)

Introduction

Cis-Diamminedichloro-platinum(II) (CDDP) is an effective anticancer agent, but tumor cells can become resistant after CDDP-based therapy (1). Detoxification of CDDP, an increase in DNA repair, and excretion of CDDP have been implicated as major factors contributing to CDDP resistance (1). Incorporated CDDP is excreted by several molecules, such as overexpressed P-glycoprotein (2), a zinc-related defense system that is regulated by increased intracellular glutathione (GSH; ref. 3), and the ATP-dependent glutathione S-conjugate export pump (GS-X pump), which plays a role in the vesicle-mediated excretion of GSH-CDDP conjugates from resistant cells (4). Recent reports suggest that minerals such as zinc (Zn) and copper (Cu), important for normal cellular functions (5), are involved in CDDP resistance (6, 7). The simultaneous monitoring of multiple numbers of cellular elements would be helpful in identifying the mechanism of drug resistance in a malignant cell. The recently developed technique of scanning X-ray fluorescence microscopy (SXFM; refs. 8, 9) has made it possible to detect elements of interest by a single measurement and give a profile of these elements at the single-cell level (termed an element array). To examine the efficacy of element array analysis, we analyzed elements before and after treatment with CDDP and compared the element profiles of CDDP-sensitive and CDDP-resistant cells. We showed that the Zn content has an inverse correlation with Pt incorporation owing to a positive linkage with glutathione (GSH), a Zn-dependent detoxification factor. The combined treatment with CDDP and *N,N,N,N*-tetrakis-(2-pyridylmethyl)-ethylenediamine (TPEN), a Zn (II)-chelator (10), increased Pt uptake with a concomitant reduction of intracellular GSH. We propose that the element array is a versatile method suitable for obtaining information about metals involved in drug metabolism and could contribute to a novel strategy for anticancer chemotherapy.

Materials and Methods

Element array analysis by scanning X-ray fluorescence microscopy. SXFM was set up at an undulator beamline, BL29XU, of the SPring-8 synchrotron radiation facility (11) by combining a Kirkpatrick-Baez–type X-ray focusing system (12, 13), an XY-scanning stage for sample mounting, and an energy-dispersive X-ray detector (SDD, Röntec, Co., Ltd.). Monochromatic X-rays at 15 keV for Pt *L*-line excitation were focused into a 1.5 μm (*H*) × 0.75 μm (*W*) spot with a measured flux of ~ 1×10^{11} photons/s. The focused X-rays simultaneously yielded the fluorescence of various chemical species in a small volume of sample cells, as shown in Fig. 1*A*. The fluorescence from each element was taken independently and did not overlap except for the Pt$L\alpha$ signal, which was contaminated by Zn$K\beta$ (Fig. 1*A*). This was corrected by subtraction, as described previously (8). In this study, we could also measure Pt$L\beta$ as a unique signal of Pt (Fig. 1*A*). After counts were collected for 4.0 to 8.5 seconds at each pixel of scanning, the detected counts were normalized by incident beam intensity. In addition to the mapping images, an elemental concentration per single cell was calculated from the integrated elemental intensity over the whole mapping image.[10]

Requests for reprints: Yukihito Ishizaka, Department of Intractable Diseases, International Medical Center of Japan, 1-21-1 Toyama, Shinjuku-ku, 162-8655 Tokyo, Japan. Phone/Fax: 81-3-5272-7527; E-mail: zakay@ri.imcj.go.jp.

[10] A. Saito et al., manuscript in preparation.

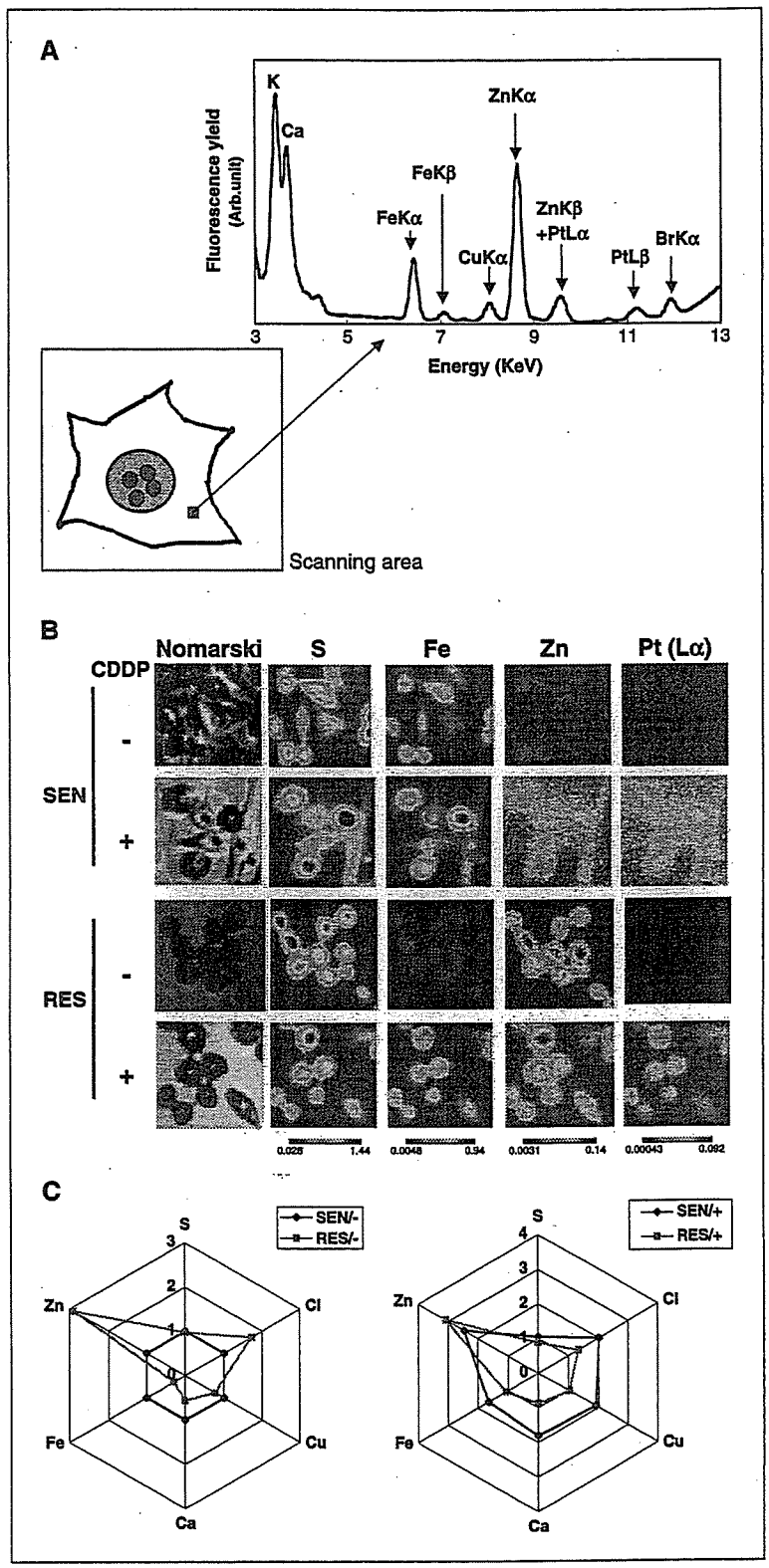

Figure 1. Element array by SXFM. *A*, scheme of imaging cellular elements by SXFM. Coherent X-rays are focused on each area (*pixel*), and the X-ray fluorescence from each element is detected. Each pixel gives an elemental spectrum, as shown in the right panel, and an integrated intensity of the individual element was mapped to the corresponding area of analyzed cells. *B*, SXFM analysis after CDDP treatment. Cell morphologies obtained by Nomarski are shown at ×100 magnification (*left*). Each field of view is equivalent to an area of 70 × 70 μm. Representative results are shown. Brighter colors indicate a higher signal intensity of each element. Results are shown for PC/SEN (*top*) and PC/RES cells (*bottom*). Note the high intensity of Pt*Lα* in PC/SEN cells after CDDP treatment (*second panel of the Pt column*) and the higher signal intensity of Zn in PC/RES cells compared with that of PC/SEN cells. *C*, element array based on SXFM analysis. The mean signal intensity of each element obtained by SXFM analysis was calculated, and the fold increase of elements in PC/RES cells (*red*) was depicted by using the intensity in PC/SEN cells (*blue*) as a standard (*left*). A part of analyzed elements is shown. The fold increase of elements in PC/SEN (*blue*) and PC/RES cells (*red*) after CDDP treatment was also shown by using the intensity in PC/SEN before CDDP treatment as a standard (*right*).

Chemicals and biochemical assays. TPEN (Sigma, St. Louis, MO; ref. 10), GSH (Calbiochem, La Jolla, CA), and CDDP (Daiichi Kagaku, Tokyo, Japan) were purchased. A GSH colorimetric assay kit (Calbiochem) and a BCA protein assay kit (Bio-Rad, Hercules, CA) were used for measuring intracellular GSH. About 3×10^5 to 4×10^5 cells were subjected to GSH measurement, and the data were normalized by cell number.

Cell lines. PC-9 cells (PC/SEN) and PC-9 cells resistant to CDDP (PC/RES), originally derived from a lung carcinoma cell line (14), were

maintained in DMEM (Nissui, Co., Tokyo, Japan) supplemented with 10% FCS (Sigma). The viability of PC/SEN cultured for 72 hours in the presence of 1 μmol/L CDDP was 40%, whereas that of PC/RES was ~90%. In this study, each cell line when treated with 1 μmol/L CDDP for 24 hours showed >85% viability.

Colony formation. After treatment, aliquots of PC/SEN and PC/RES were plated into culture dishes or soft agar, and the numbers of cell aggregates consisting of >50 cells were counted. Each number was normalized by plating efficiency, and the mean and SD of the number of formed colonies were calculated.

Sample preparation. Cells were plated on a silicon nitride base (NTT Advanced Technology, Tokyo, Japan) 1 day before the experiment. After incubation for 24 hours in the presence of 1 μmol/L CDDP, the cells were washed with PBS, fixed in 2% paraformaldehyde in PBS for 10 minutes at room temperature, and incubated in cold 70% ethanol for 30 minutes. The cells were then placed in a 1:3 solution of glacial acetic acid and methanol for 10 minutes, washed with 70% alcohol, and dried overnight at room temperature.

Measurement of cellular platinum and zinc. To measure Pt and Zn, ~5 × 10^6 cells were subjected to inductively coupled plasma mass spectroscopy (ICP-MS; Toray Research Center, Shiga, Japan; ref. 15).

Statistical analysis. The Pearson product-moment correlation coefficient and Student's *t* test were used to evaluate statistical significance (16).

Results and Discussion

Incorporation of platinum and element array after *cis*-diamminedichloro-platinum(II) treatment. We analyzed intracellular elements by SXFM after CDDP treatment (Fig. 1*A*). At 12 hours after treatment with 1 μmol/L CDDP, the level of Pt was increased in PC/SEN cells, whereas little increase in the Pt level was seen in PC/RES cells (Fig. 1*B*). The intensity of Pt in PC/RES cells was 2.6-fold less than that in PC/SEN cells, as confirmed by the results of ICP-MS, which indicated that the amount of Pt in PC/RES cells (5.5 fg/cell) was 3.6-fold less than that in PC/SEN cells (19.7 fg/cell). Therefore, the decreased accumulation of CDDP is likely to be responsible for resistance in PC/RES cells.

Based on the mean signal intensity obtained by SXFM, element array analysis was carried out (Fig. 1*C*). The element profile

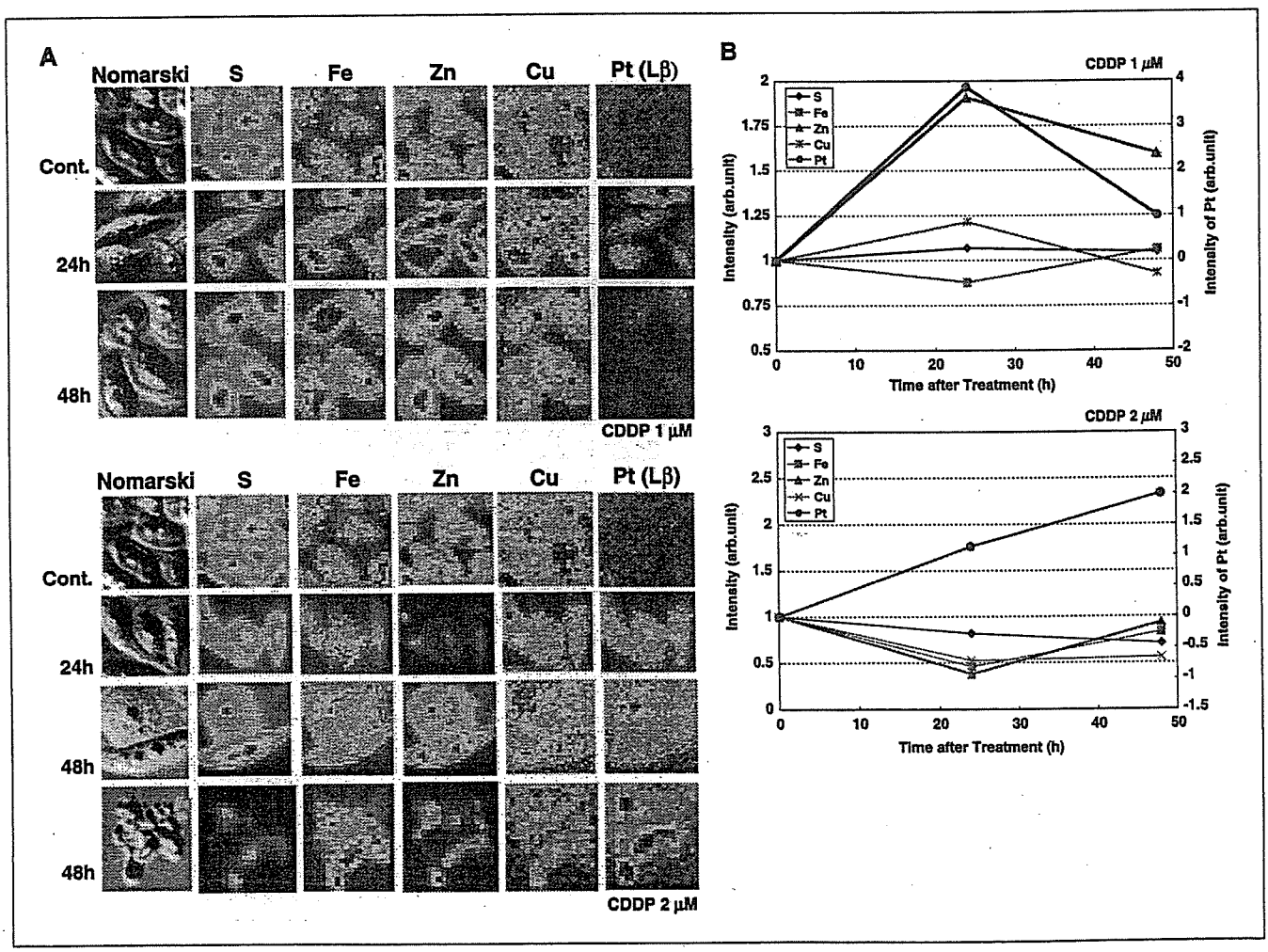

Figure 2. Chronological changes in elements after CDDP treatment. *A*, detection of elements in CDDP-treated PC/SEN cells. From the left, Nomarski images, signals of S, Fe, Zn, Cu, and Pt are shown. Top and bottom sets of panels show cells treated with 1 and 2 μmol/L CDDP, respectively. In each set of panels, control cells (*top*) and cells treated with CDDP for 24 hours (*middle*) and 48 hours (*bottom*) are shown. In this experiment, the signals of Pt*Lβ* were measured instead of Pt*Lα* (see Materials and Methods). The lowest panels show an apoptotic cell after 48 hours. *B*, summarized results of chronological changes of elements. The results after treatment with 1 μmol/L (*top*) and 2 μmol/L CDDP (*bottom*) are shown. The mean signal intensity was calculated from the results partly shown in (*A*). Among the cellular elements, Zn was most influenced by both 1 and 2 μmol/L CDDP treatment and had an inverse correlation with Pt content.

Blockade of bulky lymphoma-associated CD55 expression by RNA interference overcomes resistance to complement-dependent cytotoxicity with rituximab

Yasuhito Terui,[1,2] Takuma Sakurai,[1,3] Yuko Mishima,[1] Yuji Mishima,[2] Natsuhiko Sugimura,[2] Chino Sasaoka,[2] Kiyotsugu Kojima,[2] Masahiro Yokoyama,[1] Nobuyuki Mizunuma,[1] Shunji Takahashi,[1] Yoshinori Ito[1] and Kiyohiko Hatake[1,2,4]

[1]Division of Clinical Chemotherapy, and [2]Olympus Bio-Imaging Laboratory, Cancer Chemotherapy Center, Japanese Foundation for Cancer Research, Tokyo 135-8550, and [3]Material Research Laboratory, Morinaga Milk Industry, Zama, Kanagawa 228-8583, Japan

(Received August 29, 2005/Revised October 4, 2005/Accepted October 17, 2005/Online publication December 18, 2005)

Recently, anti-CD20 (rituximab) and anti-Her2/neu (trastuzumab) antibodies have been developed and applied to the treatment of malignant lymphoma and breast cancer, respectively. However, bulky lymphoma is known to be resistant to rituximab therapy, and this needs to be overcome. Fresh lymphoma cells were collected from 30 patients with non-Hodgkin's lymphoma, the expression of CD20 and CD55 was examined by flow cytometry, and complement-dependent cytotoxicity (CDC) assays were carried out. Susceptibility to CDC with rituximab was decreased in a tumor size-dependent manner ($r = -0.895$, $P < 0.0001$), but not in a CD20-dependent manner ($r = -0.076$, $P = 0.6807$) using clinical samples. One complement-inhibitory protein, CD55, contributed to bulky lymphoma-related resistance to CDC with rituximab. A decrease in susceptibility to CDC with rituximab was statistically dependent on CD55 expression ($r = -0.927$, $P < 0.0001$) and the relationship between tumor size and CD55 expression showed a significant positive correlation ($r = 0.921$, $P < 0.0001$) using clinical samples. To overcome the resistance to rituximab by high expression of CD55 in bulky lymphoma masses, small interfering RNA (siRNA) was designed from the DNA sequence corresponding to nucleic acids 1–380 of the CD55 cDNA. Introduction of this siRNA decreased CD55 expression in the breast cancer cell line SK-BR3 and in CD20-positive cells of patients with recurrent lymphoma; resistance to CDC was also inhibited. This observation gives us a novel strategy to suppress bulky disease-related resistance to monoclonal antibody treatment. (*Cancer Sci* 2006; 97: 72–79)

In recent years, monoclonal antibodies have been used increasingly to treat patients with malignancies such as lymphoma and breast cancer.[1–3] In particular, the anti-CD20 antibody, also called rituximab, is usually very effective for treatment of malignant lymphoma, and most patients can receive rituximab as monotherapy or combination chemotherapy.[4,5] However, in some cases with bulky mass and at stage IV, lymphoma cells become resistant to rituximab treatment.[6,7] Apart from the number of tumor cells being greater in these cases, how this resistance occurs has not yet been clarified.

Recently, some researchers have reported four mechanisms for the action of rituximab: (i) inhibition of proliferation; (ii) induction of apoptosis; (iii) complement-dependent cytotoxicity (CDC); and (iv) antibody-dependent cellular cytotoxicity (ADCC).[7,8] Because CDC could more rapidly and efficiently act on the target cells attacked by rituximab, CDC may be the most important of the mechanisms of rituximab.

The role of complementary regulatory proteins in the modulation of rituximab efficacy has been addressed, and several surface membrane proteins regulate the deposition of active complement proteins on cellular membranes to prevent cell lysis. Regulators of the complement system play an important role in CDC, and CD46, CD55 and CD59 are well known to inhibit the complement system.[9] Among these inhibitors, CD55 and CD59 seem to be the most important.[10] No differences in the expression of CD59 molecules have been reported between normal B cells and malignant B cells, whereas CD55 expression was shown to be different among individual patients with B-cell malignancy.[11] Nevertheless, *in vitro* susceptibility to rituximab-induced CDC could not be predicted by the level of these proteins in chronic lymphocytic leukemia (CLL) cells, and *in vivo* susceptibility could not be predicted in follicular lymphoma (FL) and CLL patients.[12,13] In contrast, some researchers have reported direct correlations among CDC, CD55 and CD59 using B-cell lines.[14]

CD55, also known as decay accelerating factor, is a major regulator of the alternative and classical pathways of complement activation and is expressed on all serum-exposed cells. CD55 is a 70-kDa glycoprotein, which is a glycosylphosphatidylinositol (GPI)-anchored protein.[15] CD55 can bind the complex of C3a and Bb, which is in the classical pathway, and it blocks the cascade of the complement system. A functional disorder of CD55 in blood cells causes paroxysmal nocturnal hemoglobinuria (PNH).[16] In these cases, the cascade of the complement system can not be controlled, and CDC activity is enhanced mainly against red blood cells. CD55 can enhance dissociation between C3 convertase and C4bC2/C3bBb complexes, and then inhibit the cascade of the

[4]To whom correspondence should be addressed. E-mail: khatake@jfcr.or.jp.

doi: 10.1111/j.1349-7006.2006.00139.x

complement system. While it is true that CD55 levels are low to absent in PNH, the disease is caused by phosphatidylinositol glycan-A (PIGA) gene mutations that lead to a failure to assemble GPI anchors. Hence, all GPI-anchored proteins are missing in this disease.

Previous researchers have shown that certain conditions for cancer cells, such as hypoxia, poor nutrition and bulky mass, make them chemoresistant.[17,18] When gastric cancer cells were exposed to hypoxia, hypoxia inducible factor (HIF)-1 was induced and the cells were resistant to Cis-platin (CDDP).[18] When lymphoid cells were able to resist doxorubicin (adriamycin), expression of nuclear factor (NF)-κB and its transcription activity were enhanced in doxorubicin (adriamycin)-resistant cells.[17]

Because CDC activity is especially important for rituximab therapy and CD55 may function as a mostly important inhibitor of CDC, it is possible that a decline in CDC activity by CD55 molecules may cause resistance to rituximab. CDC correlates directly with the expression of CD20 antigen in malignant B cells, and *in vitro* susceptibility to rituximab-mediated CDC depends primarily on CD20 protein expression. However, there have yet been no reports about the relationship between tumor size and sensitivity to CDC or between tumor size and CD55 expression.

More recently, small interfering RNA (siRNA) has been developed and applied to knock down target gene expression.[19] For example, the nuclear factor of activated T cells (NFAT) and NF-κB were shown to be constitutively active in large B-cell lymphoma cells, and downregulation of NFATc1 and NF-κB in malignant B-cell lymphoma with siRNA inhibited lymphoma cell growth.[20] Although many researchers tried siRNA for genes of membrane proteins such as growth factor receptors,[21] there have been no successful reports describing siRNA for complement inhibitors.

To clarify the resistance to rituximab and overcome the resistance, especially with regard to bulky mass unresponsiveness and efficacy for re-treatment, we examined the relationship between CDC activity and rituximab, and CD55 expression in our patients, using siRNA for CD55 to treat CDC with rituximab.

Materials and Methods

Cell lines

Human malignant B-cell lines as well as Daudi and Raji cells (ATCC) were cultured in RPMI-1640 (Gibco, Carlsbad, CA, USA) with 10% fetal calf serum (FCS) at 37°C. The cell lines were used as sensitive and resistant controls in CDC with anti-CD20 antibody. The human breast cancer cell lines MCF7 and SK-BR3 (ATCC) were cultured in Dulbecco's minimal essential medium (DMEM; Gibco) with 10% FCS.

Complement-mediated cytotoxicity assay

Cells were washed once with fresh complete medium, and anti-CD20 antibody (rituximab; Roche, Basel, Switzerland) or anti-Her2/neu antibody (trastuzumab; Roche) was added at a concentration of 20 μg/mL. Cells were incubated at 37°C for 1 h, and then human AB blood serum from healthy volunteers with informed consent was added at 20% (v/v). After incubation at 37°C for 1 h, propidium iodide (PI; Sigma, St Louis, MO, USA) was added and CDC assays were carried out by flow cytometry with FACscan (Becton Dickinson, San Jose, CA, USA). For CDC assays using a microplate reader, Daudi, Raji and SKBR3 cells were seeded at 1×10^5 cell/mL in each well, and then rituximab or trastuzumab (20 μg/mL) and normal AB serum (20% [v/v]) were added. The reaction was incubated at 37°C for 1 h, and the cells were washed with phosphate-buffered saline (PBS) at least three times. Ten microliters of Calcein-AM (2 μg/mL) (Dojindo, Kumamoto, Japan) was added to each well and mixed thoroughly. After incubation at room temperature, fluorescence intensity was measured at 485 nm/535 nm wavelengths with a microplate reader (Fluoroskan Ascent; Labsystems, Helsinki, Finland).

Surface markers

Cells were washed once with PBS, and were then were stained with phycoerythrin (PE)-conjugated anti-CD20, and fluoresceinisothiocyanate (FITC)-conjugated anti-CD55 (Becton Dickinson). Flow cytometry was then carried out using FACscan. The intensities of C20 and CD55 expression were normalized compared with a control. For confocal laser scanning microscopy, rituximab and trastuzumab were labeled with Alexa Fluor 594 (Molecular Probes; Invitrogen, Carlsbad, CA, USA) in accordance with the manufacturer's instructions. In brief, 100 μg of antibody was labeled with Alexa Fluor 594 for 20 min after alkalization with carbonate. The mixture was put into a spin column and spun down at 1500*g*, and the flow-through was collected as Alexa Fluor 594-conjugated antibody.

Laser scanning confocal microscopy and phase-contrast microscopy

To see CDC activity on living cells, pictures were taken by a CDC camera with phase-contrast microscopy after the CDC assay with rituximab or trastuzumab. The cells were also stained with Alexa Fluor 594-labeled rituximab or Alexa Fluor 594-labeled trastuzumab and FITC-labeled anti-CD55 antibody, and serum was added to the culture medium. The stained cells were observed in real time under a confocal laser scanning microscopy system (Olympus, Tokyo, Japan).

Collection of clinical samples

Fresh lymphoma cells were collected from the lymph nodes of 30 patients with non-Hodgkin's lymphoma (11 cases of diffuse large B-cell type, 10 cases of marginal zone cell type, five cases of follicular cell type, two cases of small lymphocytic type, one case of B-cell immunoblastic type, and one case of diffuse small cell type) after receiving informed consent. In brief, the lymph nodes were resected surgically and specimens were broken into small pieces with scissors and ground between two glass slides. The cells were collected after centrifugation and washed with RPMI-1640 containing 10% FCS. Cell counting and viability were assessed by toluidine-blue exclusion dye test, and CD19-positive cells were isolated using a magnetic cell sorting (MACS) system. The isolated cells were stained with FITC-conjugated anti-CD19, PE-conjugated anti-CD20, and FITC-conjugated anti-CD55 antibodies and flow cytometry was then carried out.

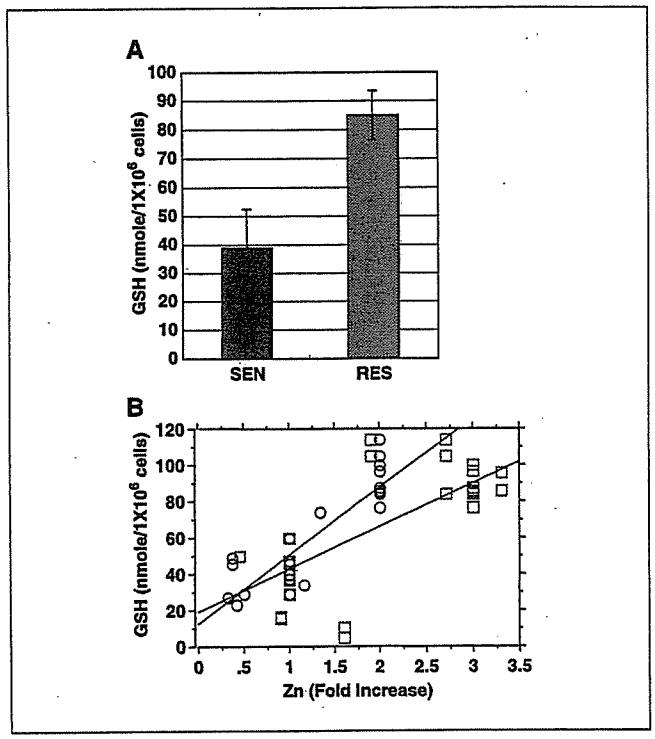

Figure 3. Cellular Zn content and GSH. *A*, basal level of intracellular GSH. The intracellular GSH levels in PC/SEN (*black*) and PC/RES cells (*gray*) were measured. GSH was significantly higher in PC/RES than in PC/SEN cells (t test, $P < 0.05$). *B*, correlation between Zn and intracellular GSH. A scatter diagram for Pearson product-moment correlation coefficient is depicted. Zn, measured by SXFM (*red squares*, $n = 27$) and by ICP-MS (*green circles*, $n = 29$), was plotted against intracellular GSH. Scattered values were based on data from both PC/SEN and PC/RES cells. The correlation coefficient r was calculated, and the statistical significance was determined ($P < 0.05$).

facilitates the identification of the elements related to the mechanism of drug resistance to CDDP. First, we noticed that the Zn content of untreated PC/RES cells was ~3-fold of that in PC/SEN cells (Fig. 1*C*, *left*). The difference in the Zn contents of these cells was confirmed by ICP-MS analysis (105 fg/cell for PC/SEN cells and 189 fg/cell for PC/RES cells, respectively). When 1 μmol/L CDDP was used for treatment, constitutive high Zn was observed in PC/RES (Fig. 1*C*, *right*). In PC/SEN cells, the amounts of all the elements were slightly increased, but the amount of Zn was increased most markedly.

We then analyzed the chronological changes in the levels of elements in PC/SEN cells following CDDP treatment. Representative results for S, Fe, Zn, Cu, and Pt are shown in Fig. 2*A*. Pt was clearly observed at 24 hours after treatment with 1 or 2 μmol/L CDDP (Fig. 2*A*). It was, however, barely detectable at 48 hours after the cells were treated with 1 μmol/L CDDP (Fig. 2*A*, *top*), suggesting that the cells excreted CDDP. In contrast, the cellular content of Pt gradually increased after treatment with 2 μmol/L CDDP (Fig. 2*A*, *bottom*), and apoptotic cells with high levels of incorporated CDDP were observed after 48 hours (Fig. 2*A*, *bottom*).

The element profile was plotted against the time after treatment with CDDP (Fig. 2*B*). When the cells were treated with 1 μmol/L CDDP, the Zn content increased remarkably and reached a peak at 24 hours (Fig. 2*B*, *top*, *red line*). In these cells, the Pt content was reduced after 48 hours. When the cells were treated with 2 μmol/L CDDP, the Zn content decreased within 24 hours (Fig. 2*B*, *bottom*), and the Pt content increased within 48 hours. In this analysis, Cu did not show significant changes. The results imply that the intracellular Zn content has an inverse correlation with the incorporated Pt content.

Cellular zinc and zinc-related detoxification. We studied Zn-related detoxification factors, such as metallothioneins (17), GSH (18), and the GSH-coupled excretory pump GS-X (4), and we observed that intracellular GSH was high in PC/RES cells (Fig. 3*A*). We then examined the possible correlation between the intracellular Zn content and GSH. As shown in Fig. 3*B*, the GSH levels showed a significant correlation with the levels of Zn detected by both ICP-MS and SXFM (Pearson product-moment correlation coefficient $r = 0.794$, $P < 0.05$ and $r = 0.533$, $P < 0.05$, respectively). The levels of Zn detected by SXFM may have less correlation with GSH than do the levels detected by ICP-MS because SXFM analyzed Zn in a small number of cells, whereas the analyses of GSH using ICP-MS were carried out on $>10^5$ cells.

Effects of zinc depletion and *cis*-diamminedichloroplatinum(II) uptake. To examine ways of increasing the sensitivity of PC/RES cells to CDDP, we used the Zn(II) chelator TPEN, as it was thought that CDDP uptake would increase when the GSH level was down-regulated by decreased Zn. Consistent with this hypothesis, treatment with 7.5 μmol/L of TPEN decreased cellular Zn to ~40 fg/cell at 30 hours after treatment in PC/SEN cells (Fig. 4*A*, *left*, *solid line*). The decrease seen in PC/RES cells owing to TPEN treatment was more rapid, with the Zn concentration being reduced to ~40 fg/cell within 7 hours (Fig. 4*A*, *left*, *dashed line*). The intracellular GSH also decreased with the reduction in intracellular Zn (Fig. 4*A*, *right*, *dashed line*).

To determine the effects of TPEN on the growth of PC/RES cells, the cells were pulse-treated for 2 hours with TPEN for 5 consecutive days and the growth was examined. Although treatment with 1 μmol/L CDDP did not induce apparent morphologic changes (Fig. 4*B*, *bottom*, *left*), the combined treatment with TPEN and CDDP caused prominent changes (Fig. 4*B*, *bottom*, *right*). A colony formation assay clearly showed that the combination of CDDP and TPEN, as well as single TPEN treatment, significantly impaired the growth of PC/RES cells (Fig. 4*C*). Consistent with these changes, ICP-MS indicated that the intracellular Pt content increased 3.5-fold after the combined treatment (from 0.38 to 1.35 fg/cell with TPEN treatment). It is important to note that the same dose of TPEN did not attenuate the growth of PC/SEN cells (Fig. 4*C*). These data indicate that the GSH level seems to be critical for resistance in PC/RES cells, consistent with previous reports that CDDP-resistant cells have high levels of GSH and that a decrease in GSH results in loss of resistance (3, 19). Our data also suggest that the high GSH content was maintained by the effects of Zn in PC/RES cells. Overall, our trial treatment with combined TPEN and CDDP suggests that this combination would be effective in eliminating tumors even if they include a CDDP-resistant population of cells with high Zn content.

We showed the use of element array analysis by SXFM to examine a mechanism of CDDP resistance. Based on element profiles, we successfully overcame CDDP resistance in PC/RES cells by using a Zn chelator that down-regulated the GSH level. Although it has been reported that Cu is a necessary factor for CDDP incorporation (7), the present work revealed that Cu was not involved in PC/RES cells. It is tempting to speculate that drug resistance is generated by various elements, and we propose that an element array can contribute to better understanding of cancer biology as well as other fields of medical science.

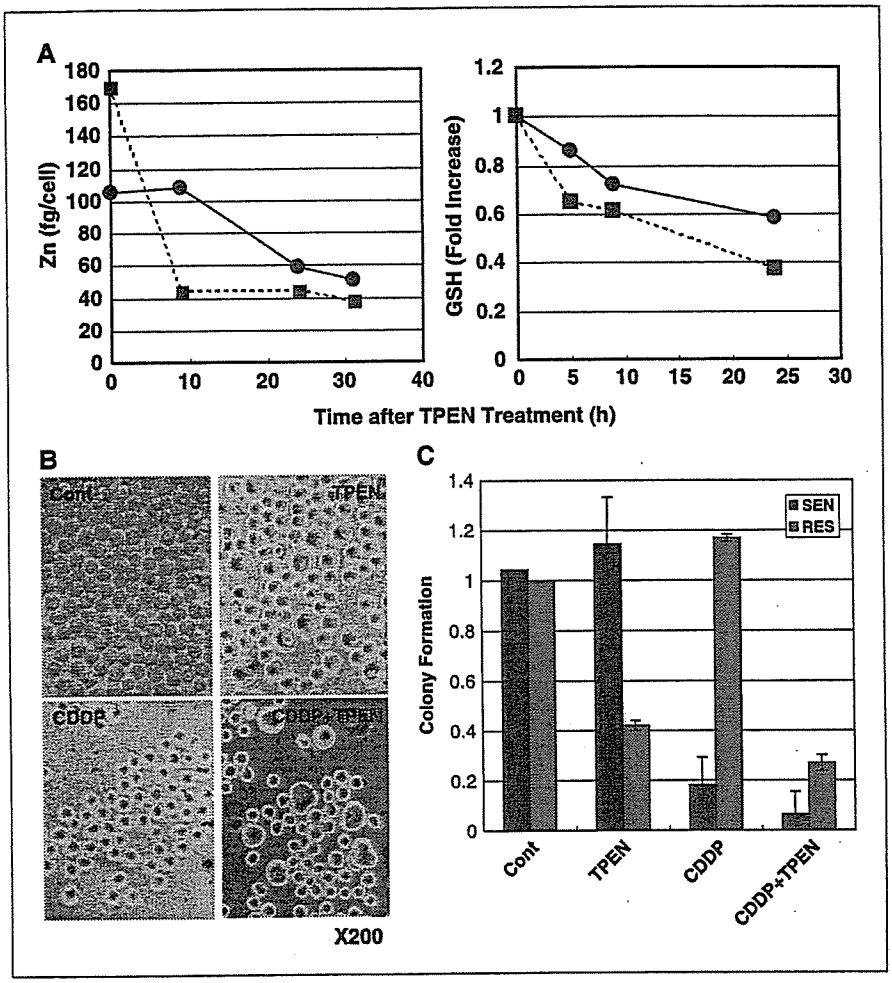

Figure 4. Cellular Zn content and Pt uptake with TPEN. *A*, TPEN-induced depletion of cellular Zn and down-regulation of GSH. TPEN (7.5 μmol/L) was added to the culture medium for the indicated time periods, and cellular Zn was measured by ICP-MS (*left*). Intracellular GSH content was also monitored (*right*). The Zn contents in PC/SEN (*solid lines*) and PC/RES cells (*dashed lines*) are shown. *B*, morphologic changes after pulse treatment with TPEN and CDDP. The morphologies of untreated PC/RES cells (*top*, *left*) and of cells treated with TPEN (*top*, *right*), CDDP (*bottom*, *left*), and CDDP plus TPEN (*bottom*, *right*) are shown. The cells were exposed to 1.0 μmol/L CDDP with or without 7.5 μmol/L TPEN for 2 hours, and then the medium was replaced with fresh medium. Pulse treatment was carried out for 5 consecutive days. Magnification, ×200. Note that large cells are observed after treatment with TPEN alone, and larger cells with irregular shape are observed following the combination treatment. The data showed that TPEN caused cellular accumulation at G_2-M phase with mitotic failure (data not shown). *C*, colony formation after pulse treatment with CDDP with or without TPEN. After pulse treatment for 5 consecutive days, as described in (*B*), the cells were plated in soft agar and the colony formation assay was done. The means and SDs of colony numbers of PC/SEN (*black columns*) and PC/RES cells (*gray columns*) are shown. The experiments were carried out in triplicate.

Acknowledgments

Received 2/3/2005; accepted 4/20/2005.

Grant support: Grant-in-aid for scientific research from the Ministry of Health, Labor, and Welfare of Japan and grant-in-aid for Center of Excellence Research (grant 08CE2004) from the Ministry of Education, Sports, Culture, Science, and Technology of Japan. The usage of BL29XU of the SPring-8 was supported by RIKEN.

The costs of publication of this article were defrayed in part by the payment of page charges. This article must therefore be hereby marked *advertisement* in accordance with 18 U.S.C. Section 1734 solely to indicate this fact.

We thank Harumi Shibata and Yasunori Suzuki for technical assistance.

References

1. Boulikas T, Vougiouka M. Cisplatin and platinum drugs at the molecular level. Oncol Rep 2003;10:1663–82.
2. Kuo TH, Liu FY, Chuang CY, Wu HS, Wang JJ, Kao A. To predict response chemotherapy using ^{99m}technetium tetrofosmin chest images in patients with untreated small cell lung cancer and compare with p-glycoprotein, multidrug resistance related protein-1, and lung resistance-related protein expression. Nucl Med Biol 2003;30:627–32.
3. Godwin AK, Meister A, O'Dwyer PJ, Huang CS, Hamilton TC, Anderson ME. High resistance to cisplatin in human ovarian cancer cell lines is associated with marked increase of glutathione synthesis. Proc Natl Acad Sci U S A 1992;89:3070–4.
4. Ishikawa T, Wright CD, Ishizuka H. GS-X pump is functionally overexpressed in *cis*-diamminedichlroroplatinum (II)-resistant human leukemia HL-60 cells and down-regulated by cell differentiation. J Biol Chem 1994;269:29085–93.
5. Mayes PA, Nutrition. In: Murray RK, Granner DK, Mayers PA, Rodwell VW, editors. Harper's biochemistry. Chapter 54. 25th ed. New York: McGraw-Hill; 2000. p. 653–61.
6. Koropatnick J, Pearson J. Zinc treatment, metallothionein expression, and resistance to cisplatin in mouse melanoma cells. Somat Cell Mol Genet 1990;16:529–37.
7. Katano K, Kondo A, Safaei R, et al. Acquisition of resistance to cisplatin is accompanied by changes in the cellular pharmacology of copper. Cancer Res 2002;62:6559–65.
8. Ilinski P, Lai B, Cai Z, et al. The direct mapping of the uptake of platinum anticancer agents in individual human ovarian adenocarcinoma cells using a hard X-ray microprobe. Cancer Res 2003;63:1776–9.
9. Hall MD, Dillon CT, Zhang M, et al. The cellular distribution and oxidation state of platinum(II) and platinum(IV) antitumor complexes in cancer cells. J Biol Inorg Chem 2003;8:726–32.
10. Parat M-O, Richard M-J, Meplan C, Favir A, Béani J-C. Impairment of cultured cell proliferation and metallothionein expression by metal chelator *NNN' N'*-tetrakis-(2-pyridylmethyl)ethylene diamine. Biol Trace Elem Res 1999;70:51–68.
11. Miao J, Hodgson KO, Ishikawa T, Larabell CA, LeGros MA, Nishino Y. Imaging whole *Escherichia coli* bacteria by using single-particle X-ray diffraction. Proc Natl Acad Sci U S A 2003;100:110–2.
12. Kirkpatrick P, Baez AV. Formation of optical images by X-rays. J Opt Soc Am 1948;38:766–74.
13. Yamauchi K, Yamamura K, Mimura H, et al. Two-dimensional submicron focusing of hard X-rays by two elliptical mirrors fabricated by plasma chemical vaporization machining and elastic emission machining. Jpn J Appl Phys 2003;42:7129–34.
14. Kawamura-Akiyama Y, Kusaba H, Kanzawa F, Tamura T, Saijo N, Nishio K. Non-cross resistance of ZD0473 in acquired cisplatin-resistant lung cancer cell lines. Lung Cancer 2002;38:43–50.
15. Richarz AN, Wolf C, Bratter P. Determination of protein-bound trace elements in human cell cytosols of different organs and different pathological states. Analyst 2003;128:640–5.
16. Glantz SA. How to test for trends. In: Glantz SA, editor. Primer of biostatistics. Chapter 8. 2nd ed. New York: McGraw-Hill; 1987. p. 191–244.
17. Jourdan E, Jeanne RM, Régine S, Pascale G. Zinc-metallothinein genoprotective effect is independent of the glutathione depletion in HaCaT keratinocytes after solar light irradiation. J Cell Biochem 2004;92:631–40.
18. Parat M-O, Richard M-J, Béani J-C, Favier A. Involvement of zinc in intracellular oxidant/antioxidant balance. Biol Trace Elem Res 1997;60:187–204.
19. Hamaguchi K, Godwin AK, Yakushiji M, O'Dwyer PJ, Ozols RH, Hamilton TC. Cross-resistance to diverse drugs is associated with primary cisplatin resistance in ovarian cancer cell lines. Cancer Res 1993;53:5225–32.

Vector and siRNA for CD55

CD55 cDNA in Ultimate open reading frame (ORF) clones (clone *ID*: IOH3209) was purchased from Invitrogen, and amplified by polymerase chain reaction (PCR) (forward, 5′-CGCGGATCCGCGATGACCGTCGCGCGG-3′; and reverse, 5′-TCCCCCGGGGGACTAAGTCAGCAAGCC-3′). The PCR product was subcloned into the pEGFP-C1 vector (Clontech, Mountain View, CA, USA). To generate double-stranded RNA for CD55, three parts of the DNA sequence, corresponding to nucleic acids 1–380, 381–817 and 821–1146 in the CD55 cDNA, were amplified by PCR. These sequences were named CD55-N, CD55-M and CD55-C, respectively. RNA transcription was then performed with this DNA template to generate sense and antisense single-stranded RNA. After production of double-stranded RNA, a reaction with the Dicer enzyme was carried out using a BLOCK-iT Dicer RNAi kit (Invitrogen). For siRNA for CD55, the siRNA was transfected into Raji and SK-BR3 cells using Lipofectamine 2000 (Invitrogen). In brief, 0.75 ng of siRNA and 5 μL of Lipofectamine 2000 in Optimen medium were mixed and incubated at room temperature for 20 min. The mixture was added to culture medium with SK-BR3 cells and fresh lymphoma cells, and the cells were incubated at 37°C for 72 h and 24 h, respectively. To see downregulation of CD55 expression, the CD55-transfected cells were stained with FITC-conjugated anti-CD55 antibody, and then expression of CD55 was observed without fixation of the cells at the same intensity of emission and excision as under laser scanning confocal fluorescent microscopy.

Statistical analysis

Correlation of susceptibility to CDC with tumor size, CD20 expression and CD55 expression were tested using the Spearman rank correlation coefficient. Statistical comparisons were carried out using two-sided Student's *t*-tests. All statistical analyses were performed using StatView 5.0 software (SAS Institute, Cary, NC, USA).

Results

Negative correlation between tumor size and susceptibility to CDC with rituximab

Rituximab is known to be effective at the early stages of indolent and aggressive lymphomas, but the effect of rituximab declines in some patients with bulky disease and a large number of lymphoma cells. According to this fact, we investigated whether susceptibility to CDC is dependent on the size of the tumor. The diameter of extirpated lymph nodes, CDC assay and CD20 expression were examined in fresh samples from 30 patients with lymphoma, as described in 'Materials and Methods'. As shown in Fig. 1a, the relationship between susceptibility to CDC and size of extirpated lymph nodes showed a significant negative correlation ($R = -0.895$, $P < 0.001$). In contrast, the relationship between susceptibility to CDC and CD20 expression, and between size of extirpated lymph nodes and CD20 expression, did not reveal significant correlations, as shown in Fig. 1b,c ($R = -0.076$, $P = 0.6807$ and 0.072, $P = 0.6979$, respectively). This suggests that susceptibility to CDC is dependent on the size of the lymphoma tumor, and that expression of CD20 does not contribute to susceptibility to CDC with rituximab in non-Hodgkin's lymphoma.

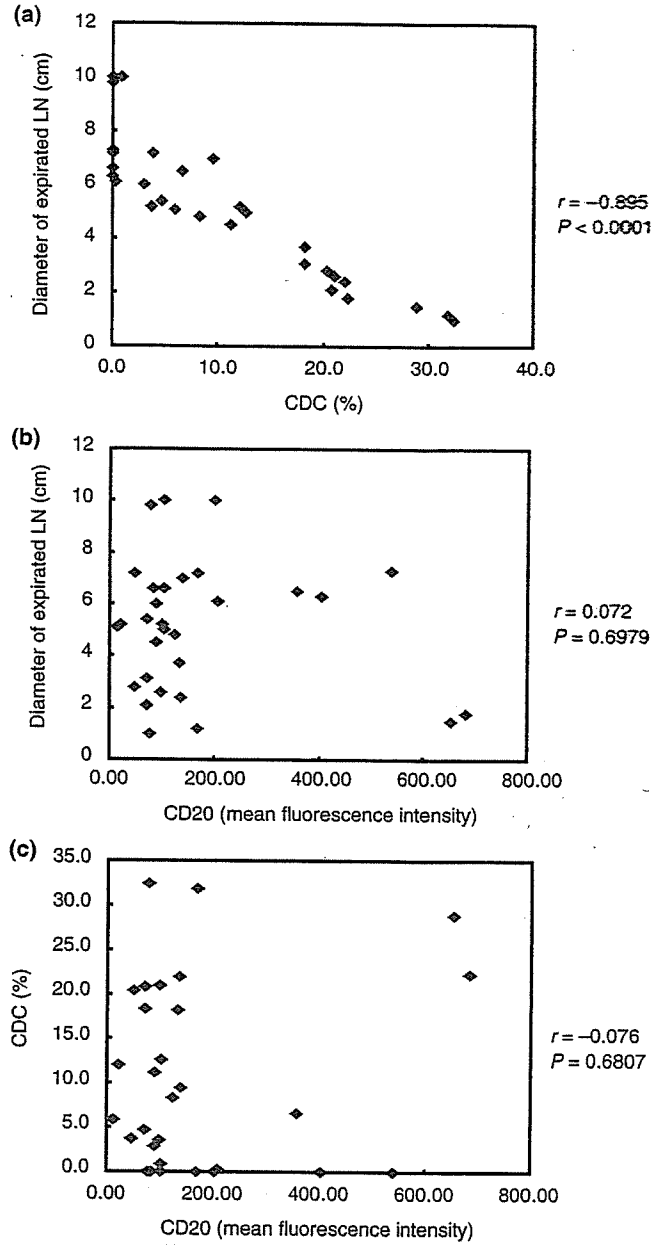

Fig. 1. Relationships between the size of extirpated tumors, susceptibility to complement-dependent cytotoxicity (CDC), and CD20 expression. The size of tumors from 30 patients with non-Hodgkin's lymphoma was measured and the cells were collected. After isolation of CD19-positive cells, FACScan analysis was carried out with anti-CD20 antibody, and CDC assay with rituximab was performed. Intensity of CD20 expression was normalized compared with a control. (a) Scatter plot and correlation analysis for size of extirpated tumor versus susceptibility to CDC. (b) Scatter plot and correlation analysis for size of extirpated tumor versus mean fluorescence intensity of CD20. (c) Scatter plot and correlation analysis for mean fluorescence intensity of CD20 versus susceptibility to CDC. All correlations were tested using the Spearman rank correlation coefficient.

doi: 10.1111/j.1349-7006.2006.00139.x

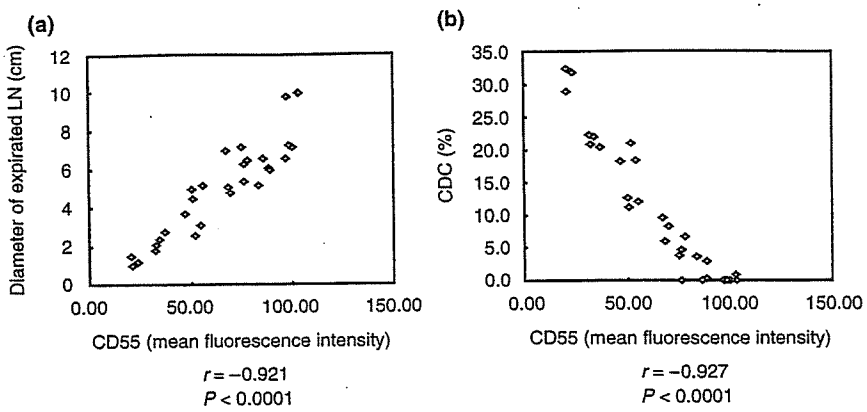

Fig. 2. Relationships between tumor size, CD55 expression and susceptibility to complement-dependent cytotoxicity (CDC). The size of tumors from 30 patients with lymphoma was measured and the cells were collected. After isolation of $CD19^+/CD20^+$ cells, FACscan analysis for CDC assay and CD55 expression were carried out. The intensity of CD55 expression was normalized compared with a control. (a) Scatter plot and correlation analysis for size of extirpated tumors versus CD55 expression. (b) Scatter plot and correlation analysis for CD55 expression versus susceptibility to CDC. All correlations were tested using the Spearman rank correlation coefficient.

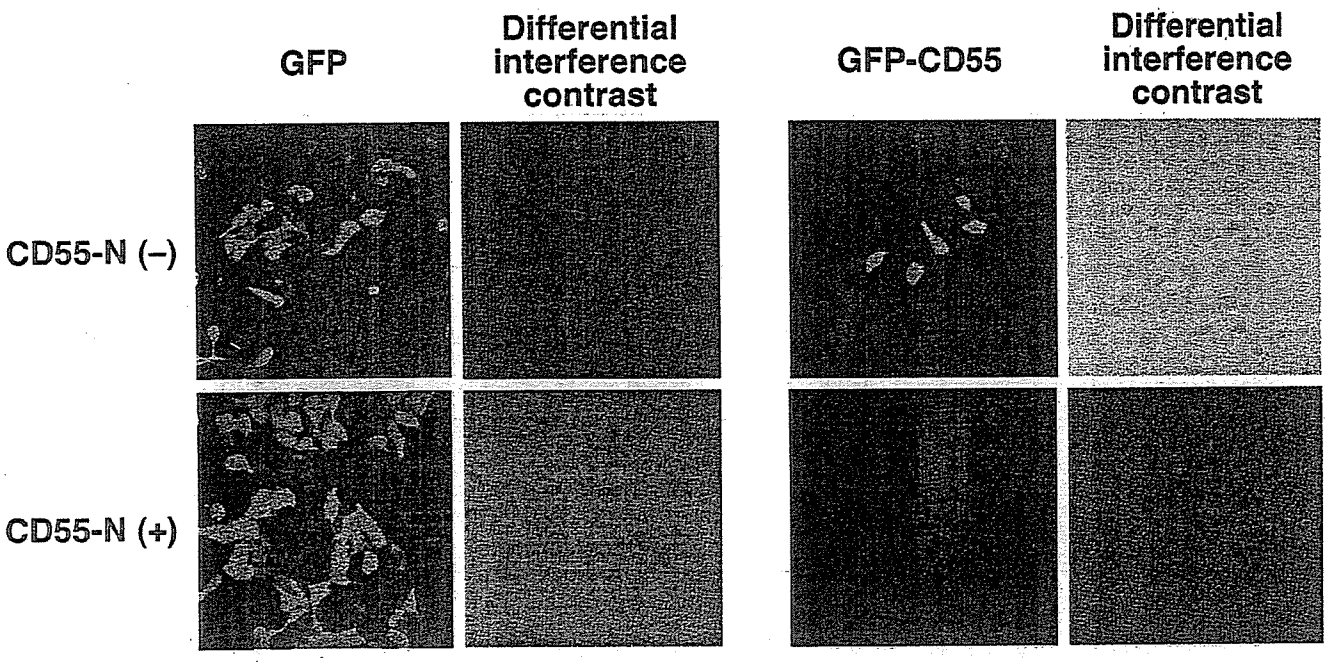

Fig. 3. Effect of small interfering RNA (siRNA) against the 5′-site of the *CD55* gene on expression of the exogenous *CD55* gene. MCF7 cells were transfected with pEGFP or pEGFP-CD55 in the presence or absence of siRNA. After 24 h, the cells were observed by laser scanning microscopy.

Size, CD55 expression and CDC in clinical samples

To investigate the relationship between the size of the extirpated tumor and CD55 expression in clinical samples, correlations between the size of extirpated tumor and fluorescence mean intensity of CD55, and between susceptibility to CDC with rituximab and fluorescence mean intensity of CD55, were analyzed statistically (Fig. 2). As shown in Fig. 2a, the level of CD55 expression on lymphoma cells was statistically correlated with the size of the lymph node ($r = 0.921$, $P < 0.001$). In contrast, the relationship between susceptibility to CDC with rituximab and fluorescence mean intensity of CD55 statistically revealed a negative correlation ($r = -0.927$, $P < 0.001$) (Fig. 2b). This suggests that increasing size of tumor contributes to higher or enhanced CD55 expression and resistance to CDC with rituximab.

Effect of siRNA for CD55 on CD55-transfected MCF7 cells

To overcome the resistance to CDC with rituximab on bulky mass, siRNA against a part of CD55 (CD55-N for 1–380 nucleotides) was designed and cotransfected with the pEGFP or pEGFP-CD55 plasmid into MCF7 cells (Fig. 3). When the cells were cotransfected with both pEGFP and siRNA for CD55, the expression of green fluorescent protein (GFP) did not change compared with transfection with only pEGFP vector (Fig. 3, upper panels). On the other hand, when the cells were cotransfected with both pEGFP-CD55 and siRNA for CD55, the expression of GFP-CD55 disappeared compared with transfection with only the pEGFP-CD55 vector (Fig. 3, lower panels). This suggests that CD55-N, siRNA against 1–380 nucleotides in the CD55 gene, is effective for blocking the expression of CD55.

Decrease in CD55 expression by siRNA overcomes resistance to CDC in breast cancer cell line SK-BR3

We investigated the use of a monoclonal antibody against the Her2/neu molecule for breast cancer, named trastuzumab.